Available online at www.sciencedirect.com

ScienceDirect

Energy Procedia 00 (2017) 000–000

Energy Procedia

www.elsevier.com/locate/procedia

13th International Conference on Greenhouse Gas Control Technologies, GHGT-13, 14-18 November 2016, Lausanne, Switzerland

Categorization of Norwegian Continental Shelf formations in terms of geological CO_2 storage potentials

Rebecca Allen[a,*], Halvor M. Nilsen[a], Odd Andersen[a], Knut-Andreas Lie[a]

[a]*SINTEF ICT, Applied Mathematics, PB 124 Blindern, 0341 Oslo, Norway*

Abstract

In the present study, we use data published alongside the Norwegian Petroleum Directorate (NPD) storage atlases to further investigate the storage capacity of 23 formations found in the Norwegian Continental Shelf. Our goal is to categorize the formations according to the main limiting factors for long-term geologic storage of CO_2. We conduct the study by defining reasonable injection scenarios and running simulations on grids constructed from the NPD data, which also include the associated averaged rock properties. The use of vertical-equilibrium models allows us to rapidly run a large number of long-term simulations of injection and migration scenarios. The ability to run rapid simulations allows us to optimize injection rates using an adjoint-based nonlinear optimization algorithm. For a given number of wells and set of boundary conditions, we aim to optimize the amount of CO_2 injected, subject to limits on long-term leakage and maximum allowed pressures. The outcome allows us to determine whether an aquifer is restricted mainly by long-time leakage across open boundaries, or global pressure buildup. We also provide figures for how much CO_2 can be injected before the limitation is reached, subject to the working assumptions and demonstrate how changing these assumptions may influence the result. In particular, the assumed injection time and cost of leakage is discussed.

We emphasize that through this study we wish to demonstrate a practical approach to the estimation of realizable storage capacity and illustrate how site-specific operational limitations influence the exploitable storage volume as compared with the initial storage estimates provided by NPD. As the study is based on large-scale averaged data under several simplifying assumptions, the realized storage capacity for each formation may well change if more detailed information, in particular on heterogeneity or more complex fluid-rock interactions, were to be taken into account. However, the use of simplified models to identify realizable storage capacity on the large scale allows us to quickly identify which formations may be best suited for a particular injection scenario.

Peer-review under responsibility of the organizing committee of GHGT-13.

Keywords: Geological CO_2 storage; Dynamic storage efficiency; Optimization; Storage categorization

* Corresponding author.
E-mail address: rebecca.allen@sintef.no

Peer-review under responsibility of the organizing committee of GHGT-13.

1. Introduction

When saline aquifers are considered for CO_2 storage, basic capacity estimates are commonly computed by combining volumetric data with a set of efficiency factors, i.e.,

$$M_{\mathrm{co2}} = S_{\mathrm{eff}} \rho_{\mathrm{co2}} V_p, \tag{1}$$

where M_{co2} is the storage capacity (in terms of mass), S_{eff} is the so-called storage efficiency factor, ρ_{co2} is the density of CO_2 at reservoir conditions, and V_p is the formation's pore volume that is deemed suitable for storage [1]. The storage efficiency factors can be obtained by combining geological and laboratory measurements, past experience, and statistical techniques based on simplifying assumptions on the injection process. Consequently, efficiency factors can be provided in tabular form and be broadly applied across a wide range of candidate formations. The range of S_{eff} reported in literature is 1.5–3.6% for open systems, and 0.3–1.2% for closed systems [2] (open and closed refers to whether the formation is in communication with neighboring formations, i.e., whether fluid is able to pass in or out of the formation).

Storage estimates computed by (1) are useful in the production of inventories on a regional or national level. CO_2 storage atlases and studies have estimated the capacity of formations located world-wide, e.g., in the USA [1], Canada [3], Australia [4], South Africa [5], Ireland [6], the UK [7,8], and Nordic regions [9–11]. In particular, the Norwegian Petroleum Directorate (NPD) issued a storage atlas of the Norwegian North Sea in 2011, later followed by similar atlases for the Norwegian Sea and the Barents Sea; see [9]. In these publications, NPD presents a large number of subsea geological formations considered as potential candidates for CO_2 storage operations, provides information on geology, and basic estimates on pore volume, storage efficiency and maturity. On the other hand, it should be noted that the basic approach of combining volumetric data and efficiency factors does not capture temporal aspects or other practical legal or economical constraints that are important when defining actual exploitation strategies. Concerns about local or global pressure buildup, as well as leakage risk associated with short-term advection or long-term migration, need to be properly taken into account when planning how much of the available storage volume can be exploited in a practical use case.

In this work, we use the formation datasets released as part of NPD's CO_2 storage atlas, to demonstrate a workflow of obtaining dynamic storage capacity estimates of the formations and their corresponding storage efficiency factors. Figure 1 shows the 23 formations that are investigated in this work. Table 1 presents volumetric storage capacities published in [9] and [10], including the assumed storage efficiency factors. The storage capacity estimates reported by [9] and [10] differ greatly for the same formation due to the portion of the formation (i.e., pore volume) under consideration. For example, in [9], only a portion of the Utsira–Skade formation was considered suitable for storage, thus the pore volume used in the calculation was much less than the pore volume used by [10]. In addition to basic (i.e, volumetric) capacity estimates, dynamic estimates have been reported in literature for several of the formations located along the Norwegian Continental Shelf; e.g., [12–17]. Similar to volumetric capacity estimates, dynamic estimates of the same formation can vary significantly depending on the portion of the formation under consideration. For example [12] considered the entire 25 000 km^2 Utsira formation, while [13,14] considered an area of 1 600 km^2 in the southern part of Utsira–Skade, and vastly different dynamic capacities were reported. For the purposes of our work, we perform simulations using the entire pore volume of the formation datasets, since practical storage amounts will be determined by our optimization framework.

2. Methods

2.1. Well placement strategy

Well placement can be carried out automatically using an algorithm. Our *greedy* algorithm, previously explained in [18] and [19], considers the trapping structure of the formation's top surface (precomputed using a spill-point analysis) and places wells according to the best available, reachable structural-trapping capacity. The ideal location of a well is at the deepest elevation in a given catchment region that lies a certain distance from the catchment or formation boundary. The algorithm continues to place wells until either the next well's injection mass is less than 1% of the total structural capacity, or it is not possible to place any more wells while satisfying the "boundary-buffer" constraints. The

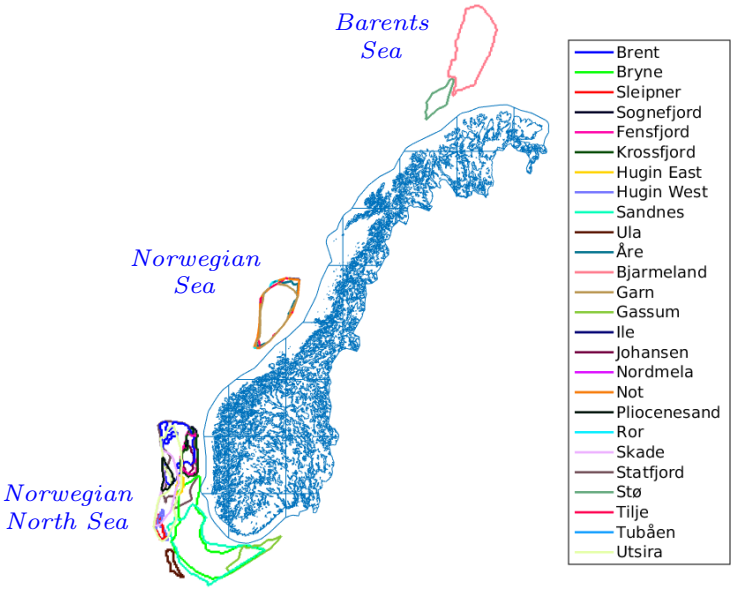

Fig. 1: Approximate location of the formations along the Norwegian Continental Shelf that are provided as publicly-available datasets by the Norwegian Petroleum Directorate. Note: sealing formations (e.g., Not and Ror), which are deemed to have low CO_2 storage potentials, are not investigated in this study.

Table 1: Volumetric capacities (in Gt) reported for NCS formations from [10] and the NPD [9]. Pore volume (V_p) is in km^3, CO_2 density (ρ_{co2}) is in kg/m^3, and storage efficiency (S_{eff}) is a percentage. Note: the Sognefjord group* includes Sognefjord, Fensfjord, and Krossfjord formations, and the capacity cited from [9] for Hugin refers to Hugin East.

	from Bøe [10]				from NPD [9]			
Formation	V_p	ρ_{co2}	S_{eff}	Capacity	V_p	ρ_{co2}	S_{eff}	Capacity
Stø–Tubåen	1164 + 748	700	2	16.296 + 13.972	120	700	3	2.5
Bjarmeland					245	650	3	4.8
Garn–Ile	540 + 448	700	2	7.560 + 6.272	300	700	0.2	0.4
Tilje–Åre	360 + 720	700	2	5.04 + 10.08	600	700	1	4.0
Brent	630	742	2	9.349				
Bryne–Sandnes	210 + 140	700	2	2.940 + 1.960	440	690	4.5	13.60
Sleipner	48	700	2	0.672				
Sognefjord Group*	180 + 180 + 90	700	2	2.520 + 2.520 + 1.260	110	690	5.5	4.09
Hugin	192	700	2	2.688	2	700	5.5	0.09
Ula	32	700	2	448				
Gassum	316	700	2	4.424	76	680	5.5	2.9
Johansen–Cook	80 + 105	700, 749	2	1.120 + 1.572	91	650	3	1.78
Utsira–Skade	918 + 349	769, 719	6	42.35 + 15.055	530	750	4	15.77
Statfjord	550	761	2	8.371	120	660	4.5	3.59

buffer distances are predefined by the user for each formation, which requires good judgment and may even require a trial and error approach until the ideal buffer distance is found. Figure 2 illustrates the location of the placed wells in each formation, and shows the initial mass to inject per well, determined from the up-slope trapping capacity. (The rate is thus the mass divided by the length of the injection time). Various buffer distances were used to place wells in each formation, but are not reported here for brevity. Some of the initial masses were reduced to ensure that the initial guess produces a non-negative objective value given a 30-year or 100-year injection period; this is to ensure that the initial guess is not too far from the global maximum of the objective function (i.e., to reduce the number of simulations required to reach convergence).

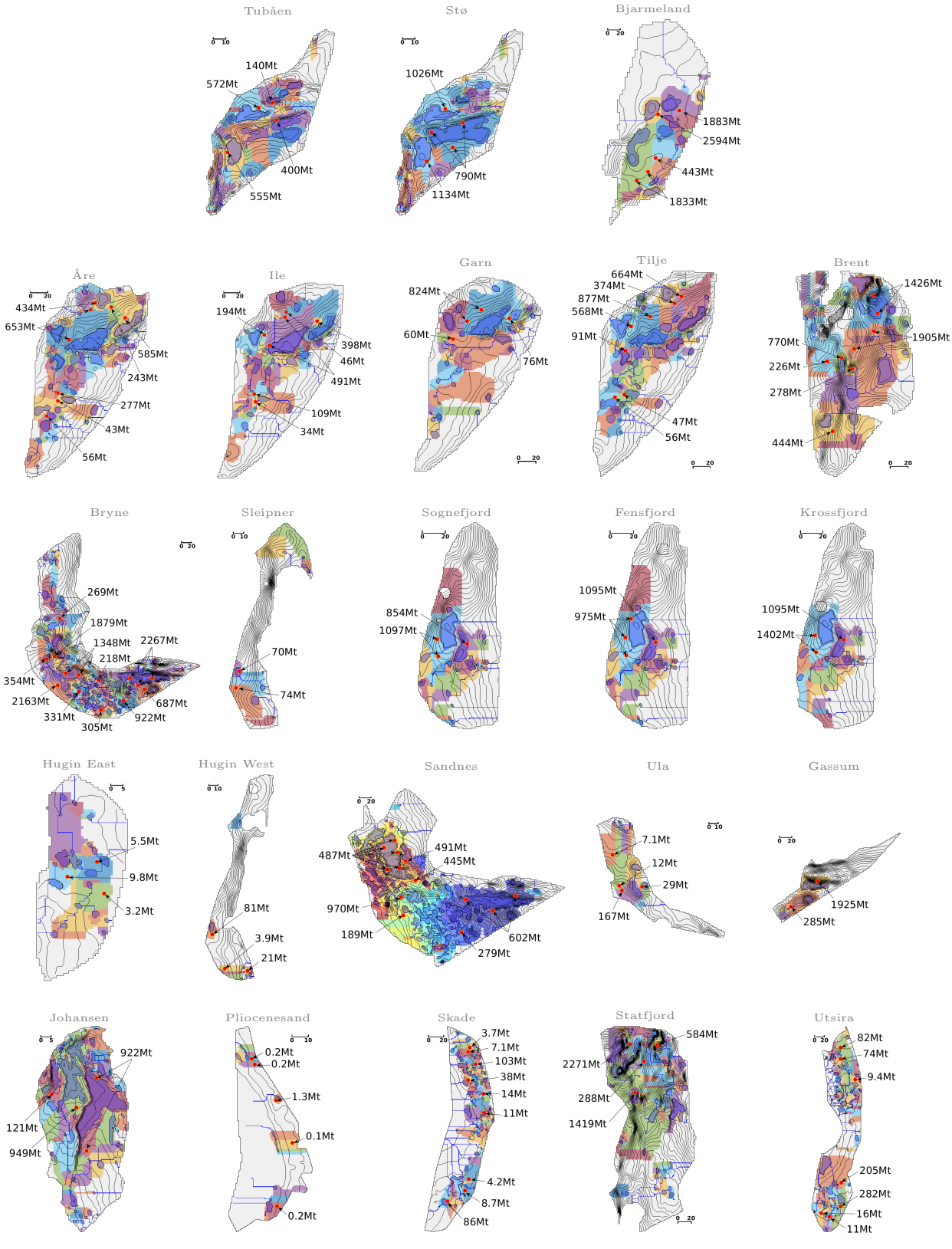

Fig. 2: Well placement and initial injection masses. Scale is indicated (in km) for each formation. Contour lines are drawn at 150 meter intervals. Wells are indicated by red dots. Color palate used for trapping structure: catchment regions are distinguished using random colors, structural traps are shown using a darker shade of its catchment region's color, and connections between traps (i.e., spill-paths) are indicated by blue lines.

2.2. Optimization of injection strategy

Once a set of wells are placed, their injection rates are optimized in order to maximize the amount of securely stored CO_2 while minimizing excess boundary leakage or pressure buildup. As such, our objective function is

$$J = M_I - C_L M_L - C_P \sum_i \left(\max\left(0, p_i - p_{i,lim}\right)\right)^2, \tag{2}$$

where M_I is the amount injected, M_L is the amount that has leaked by the end of the simulated migration period or that is forecast to leak by time infinity, p_i is the cell pressure, and $p_{i,lim}$ is the cell's predefined pressure limit. The constants C_L and C_P act to penalize CO_2 leakage and excess pressure buildup, respectively; C_L is set according to the amount of leakage that might be deemed acceptable, whereas C_P is iteratively increased until the optimal solution is one in which the pressure limit is surpassed by a tolerance of 2%. The pressure limit is assumed to be 90% of the overburden pressure, which is computed to be the weight of all fluid or media layers (i.e., sea and saturated sandstone) lying above the saline aquifer's caprock; see [20].

To find the global maximum of (2), we use the Broyden–Fletcher–Goldfarb–Shanno (BFGS) algorithm, using Wolfe conditions [21,22] with an inexact cubic line-search based on values and derivatives. The state variables (i.e., CO_2 saturation and pressure) that are required to evaluate (2) are determined via simulation. The derivatives (with respect to the state variables) are calculated using the adjoint method; see [23]. Vertical-equilibrium (VE) modeling allows us to run many rapid simulations within a manageable time frame. The underlying assumptions of VE modeling are valid for the flow dynamics of our problem: CO_2 and the formation fluid segregate into vertical layers once CO_2 is injected into the formation, due to the density difference between the fluids. Since the lateral migration of CO_2 compared to its vertical flow is orders of magnitude larger, vertical segregation is assumed to occur instantaneously. As such, the fluid flow equations can be vertically integrated and solved using a 2D grid, which drastically reduces the computational cost of solving a 3D model. Once the 2D equations are solved, the vertical distribution of CO_2 (in terms of its trapping mechanisms) are solved by analytical expressions.

The optimization method explained above, as well as variants of (2), have been applied and documented in previous work; see e.g., [19,24–27], however for select formations. Herein, we apply this method to obtain the dynamic storage efficiency of 23 of the formations available in NDP's CO_2 Storage Atlas [9].

3. Results

3.1. Categorization based on storage efficiency limitation

By applying the optimization method discussed in Sect. 2, the optimized mass to inject (M_I) is used to compute the corresponding storage efficiency (S_{eff}) according to (1). Results are shown in Figure 3. Formations are categorized based on what limited the well rates from injecting more CO_2. Most of the (open) formations are limited by leakage only, or a combination of leakage and pressure. A few formations—Bjarmeland and Sandnes—were limited purely by pressure buildup. In cases where pressure was a limiting factor, the pressure reached its predefined limit at locations surrounding an injection well (i.e., Tilje in Figure 4) or within a shallow trap (i.e., Bjarmeland in Figure 4 and Brent in top row of Figure 6). This indicates that while it is considered advantageous to place wells within the deepest regions of a formation where the overburden pressure is highest (thus the pressure limit is least restrictive), the amount to safely inject into the formation may ultimately be dictated by the maximum sustainable pressure rise that occurs in the shallowest traps where the overburden pressure is smallest.

Recall that the range of S_{eff} values reported in literature is 1.5–3.6% for open systems, and 0.3–1.2% for closed systems [2]. More specifically, the NPD have assumed that the storage efficiency of closed and partially open aquifer systems are 1% and 4–5%, respectively (excluding pressure management techniques such as brine extraction) [14]. Despite the fact that we have treated all of the formations as open systems, our dynamically-obtained storage efficiency factors reveal a similar range of values from those given by NPD [9]: S_{eff} factors in Table 1 range from 0.2 to 5.5%, whereas our estimates in Figure 3 range from 0.14 to 4.10% for a 30-year injection period, and 0.16 to 6.37% for a 100-year injection period (excluding Pliocenesand because its storage capacity is practically negligible). When values are compared for specific formations, discrepancies are evident. However, these discrepancies are not surprising

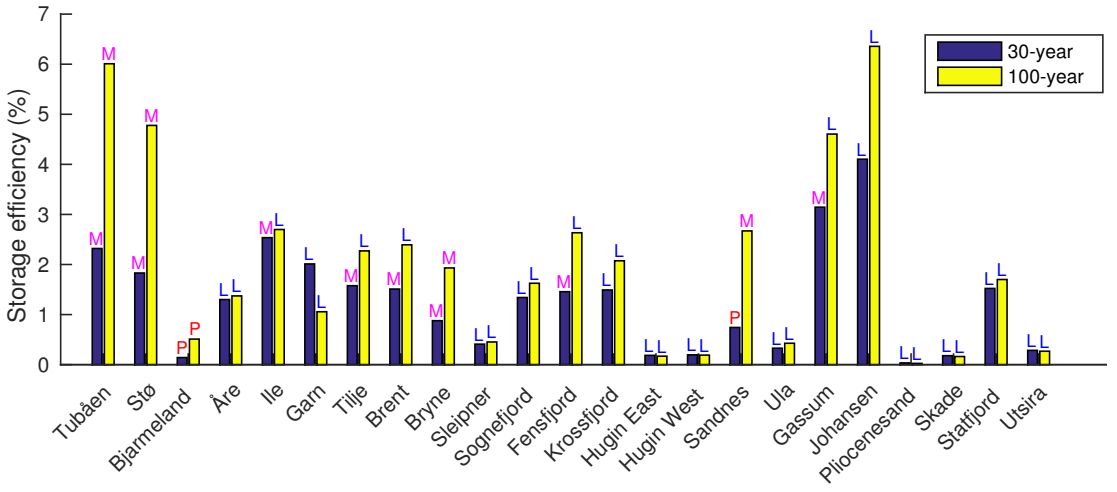

Fig. 3: Categorization of open system formations in terms of what limited their storage efficiency (S_{eff}), given two different injection time frames. S_{eff} was determined dynamically by optimizing the well injection rates and then by (1). "P" stands for pressure-limited, "L" stands for leakage-limited, and "M" stands for mixed (i.e., limitation due to a combination of pressure and leakage). Results are not intended for engineering purposes.

since we have obtained our efficiency factors dynamically, i.e., via simulations of CO_2 transport within the formation, assuming reasonable injection scenarios, and a set of working conditions which allowed for a certain amount of leakage to occur. In this regard, dynamic estimates capture temporal aspects and other important constraints (leakage, pressure buildup) that dictate the practical amount of storage volume to be exploited. Also, discrepancies are likely the result of different formation properties used, e.g., formation pore volumes, grid resolutions, constant versus depth-dependent CO_2 density, etc., and especially the role that faults could have on CO_2 migration.

3.2. Influence of working assumptions on estimating storage capacity: Injection time frame

It is important to realize that the optimized dynamic storage capacity for a given set of fixed well positions is dependent on the injection time frame. Indeed, almost all of our storage efficiency estimates changed when we lengthened the injection period from 30 to 100 years; see Figure 3. During and immediately following the injection period, the fluid flow is primarily pressure-driven, and only in the later stages of post-injection does the flow (or migration) of the CO_2 plume become solely buoyancy-driven. In a leakage-limited injection strategy, the optimal solution may include a combination of leakage occurring at different time scales. Short-term CO_2 leakage that occurs across the formation boundaries nearby the injection well will likely limit the injection rate, thus resulting in under-utilization of the spill-path's trapping potential. On the other hand, an injection rate that is limited due to long-term migration leakage is an indication that the trapping potential of the spill-path has been largely utilized; but to achieve this, the injection time needs to be a suitable length such that the injected CO_2 remains contained within the trapping structure until it migrates towards the end of the spill-path.

The fact that the storage efficiency of some formations were reduced when the injection period was lengthened indicates that there is an optimal *time frame of injection* in addition to optimal injection rates. To illustrate this more clearly, optimal solutions were found for a single-well scenario in Sleipner using injection periods of 10, 30, and 100 years; see Figure 5. From the trapping inventory of the 10-year optimal solution, we can see that most of the leakage has happened immediately following the injection period; the injection mass has been limited by *near-well leakage* due to short-term advection. Due to this type of leakage, the full trapping potential of the spill-path has not been exploited. On the other hand, the optimal solution given an injection period of 30 years does not exhibit this near-well leakage. Rather, by the end of the injection period, the CO_2 plume has migrated farther upslope and is not as concentrated around the injection well compared to the 10-year injection case. The leakage that ultimately limits the amount to inject occurs at the *end of the spill-path* due to long-term migration. In this way, more of the trapping potential of the spill-path is being exploited. It is interesting to note that the final sweep of the CO_2 plume is quite

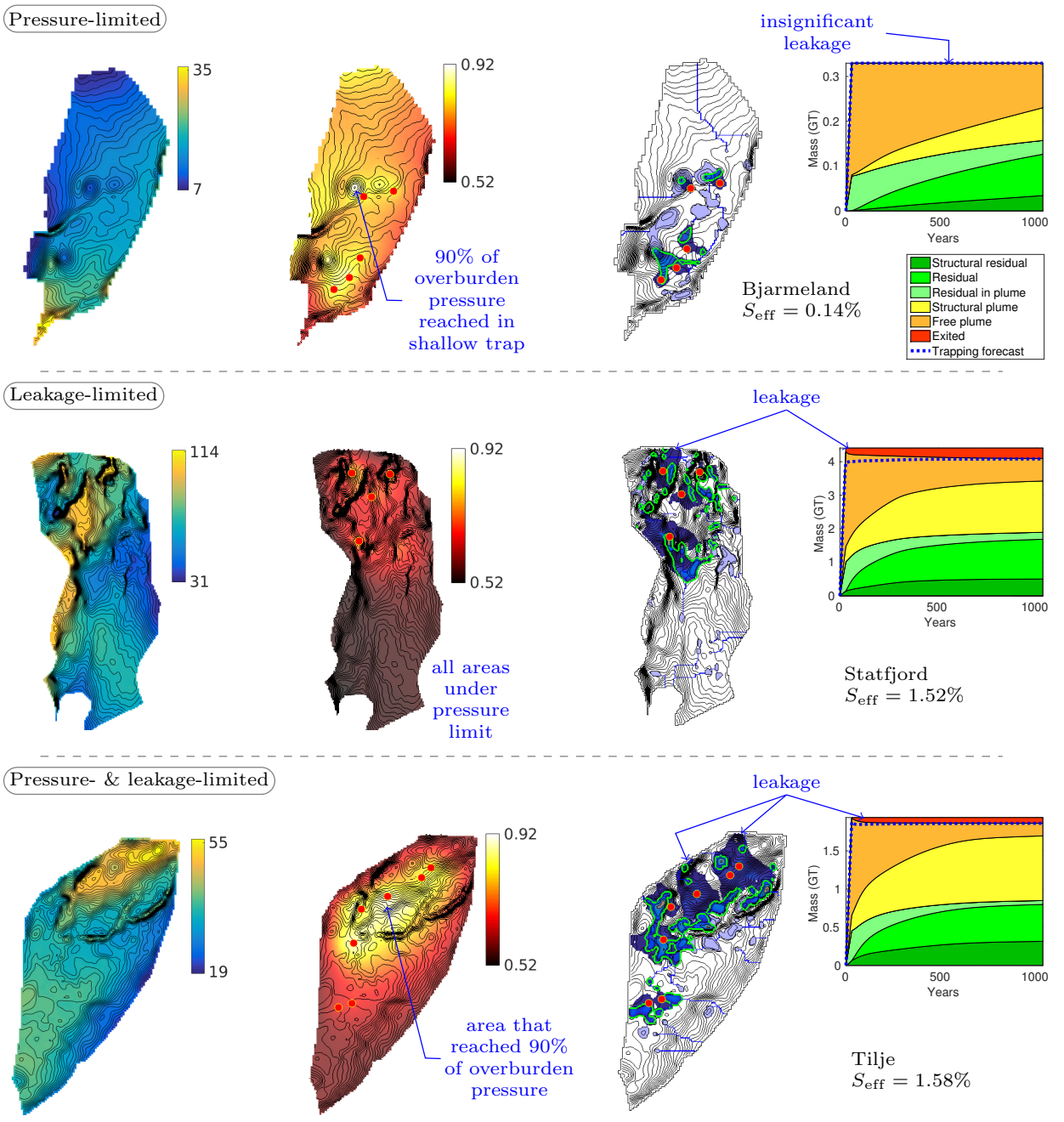

Fig. 4: Examples of three different categories of open-system injection strategies, in terms of what limited the storage efficiency. *Left to right*: overburden pressure (in MPa), fraction of overburden pressure reached, CO_2 saturation after 1000 years, and trapping inventory. Optimized examples were obtained using a 30-year injection period and a leakage penalty factor of 5. Fraction of overburden pressure reached is with respect to the entire simulation period, and indicates the locations where pressure reached or approached its pressure limit within a factor of safety. S_{eff} is storage efficiency.

similar in the 10- and 30-year optimals, and even though the amount of residually trapped CO_2 is similar, the 30-year optimal is able to exploit more structural trapping. In the 100-year optimal, the amount structurally trapped is similar to the other cases, but the injection mass is limited by the lack of residual trapping that takes place during plume migration; in this case, the sweep of the CO_2 plume is the smallest. While the optimal solution is still able to fill the

structural traps, there is a trade-off between how much more CO_2 could be residually trapped and how much more CO_2 will leak by increasing the injection mass. A low injection rate over a long injection period lacks significant pressure-driven flow. As such, the injected mass behaves more like a trickle of fluid, spilling upslope along a narrow path towards a peak of the formation, and the result is a smaller CO_2 plume sweep and much less residual trapping. Increasing the injection rate can only do so much to increase the CO_2 plume sweep and the residual trapping before "*end-of-spill-path leakage*" ultimately dictates the optimal solution.

The length of the injection period also influences the manner in which the optimal storage capacity was limited. Taking the Brent formation as an example, the storage efficiency of the 30-year optimal was limited by both pressure and leakage, whereas only leakage was the limiting factor in the 100-year optimal. This is evident in Figure 6, where approximately 90% of the overburden pressure was reached *in combination with* a noticeable amount of leakage in the 30-year optimal (top row in figure), whereas all areas remained under the pressure limit in the 100-year optimal (bottow row). It is also evident that the sweep of the CO_2 plume is smaller in the 30-year optimal than in the 100-year: this is likely the reason why more structural and residual trapping occurs in the 100-year optimal.

3.3. Influence of working assumptions on estimating storage capacity: Degree of leakage penalty

Recall that in our optimization approach, we aim to maximize the amount of securely stored CO_2 while minimizing the amount of CO_2 that leaks from the formation. In this way, we assign a penalty factor for CO_2 leakage; for example, $C = 5$ implies that leakage will be limited to less than 20% of the amount injected, $C = 30$ implies leakage will be limited to less than 3.3%, etc. Our assessment of the penalty factor's impact on storage efficiency is shown in Figure 7 for four selected formations: Bjarmeland, Fensfjord, Gassum, and Tilje. In the case of Bjarmeland, the leakage penalty factors tested here have no significant impact on the optimal storage efficiency and there is essentially no leakage under any penalty factor, even when leakage is not severely penalized (i.e., when $C_L = 3$). Since the pressure buildup reached the predefined limit, it is evident that this formation's storage efficiency is purely pressure-limited. On the other hand, the optimal injection strategies in Fensfjord, Gassum, and Tilje produce an appreciable amount of leakage in addition to reaching the pressure limit (except when leakage is severely penalized with $C_L = 30$). So, while these formations are limited by a mixture of leakage and pressure buildup, the leakage penalty factor is effective in controlling the amount of leakage permitted to occur while maximizing storage efficiency. Moreover, once leakage is severely penalized ($C_L = 30$), more of the storage efficiencies are limited due to leakage only rather than due to pressure buildup.

4. Conclusions

Our motivation was to categorize the optimized injection strategies of many different saline aquifer formations, in terms of what limited the injection of more CO_2. Given the injection periods and leakage penalty factors, as well as the particular method of well placement used in this work, we found most of the injection strategies analyzed were limited by leakage or a combination of leakage and pressure buildup. A few were limited by pressure buildup only, when the pressure reached a predefined limit (i.e., the overburden pressure multiplied by a safety factor of 0.9). By comparing the storage efficiencies given a 30-year and a 100-year injection period, it was evident that an optimal injection period length exists for each formation. We also demonstrated the impact that different leakage penalty factors have on the storage efficiencies, and showed that a purely pressure-limited formation is one in which the leakage penalty factor has no appreciable influence.

While we have presented storage efficiency factors that lie within the typically applied range for closed and open aquifer systems, we wish to emphasize that our estimates are not intended to be used for engineering purposes. Rather our intention is to demonstrate a workflow of how one can use spill-point analysis and simplified flow models to get dynamic storage estimates of various geological formations, and to categorize formations based on their storage limitations. Indeed, our categorization results also include their own limitations, given the fact that the formation datasets assumed homogeneous rock properties, neglected fine-scale details, and lacked fault information; we realize that including these important aquifer characteristics will impact the flow dynamics and presumably produce different storage efficiency factors. For example, should heterogeneous rock properties be included, fluid migration through low permeable zones will become retarded. The effect of this retardation will constrain the sweep and/or migration of

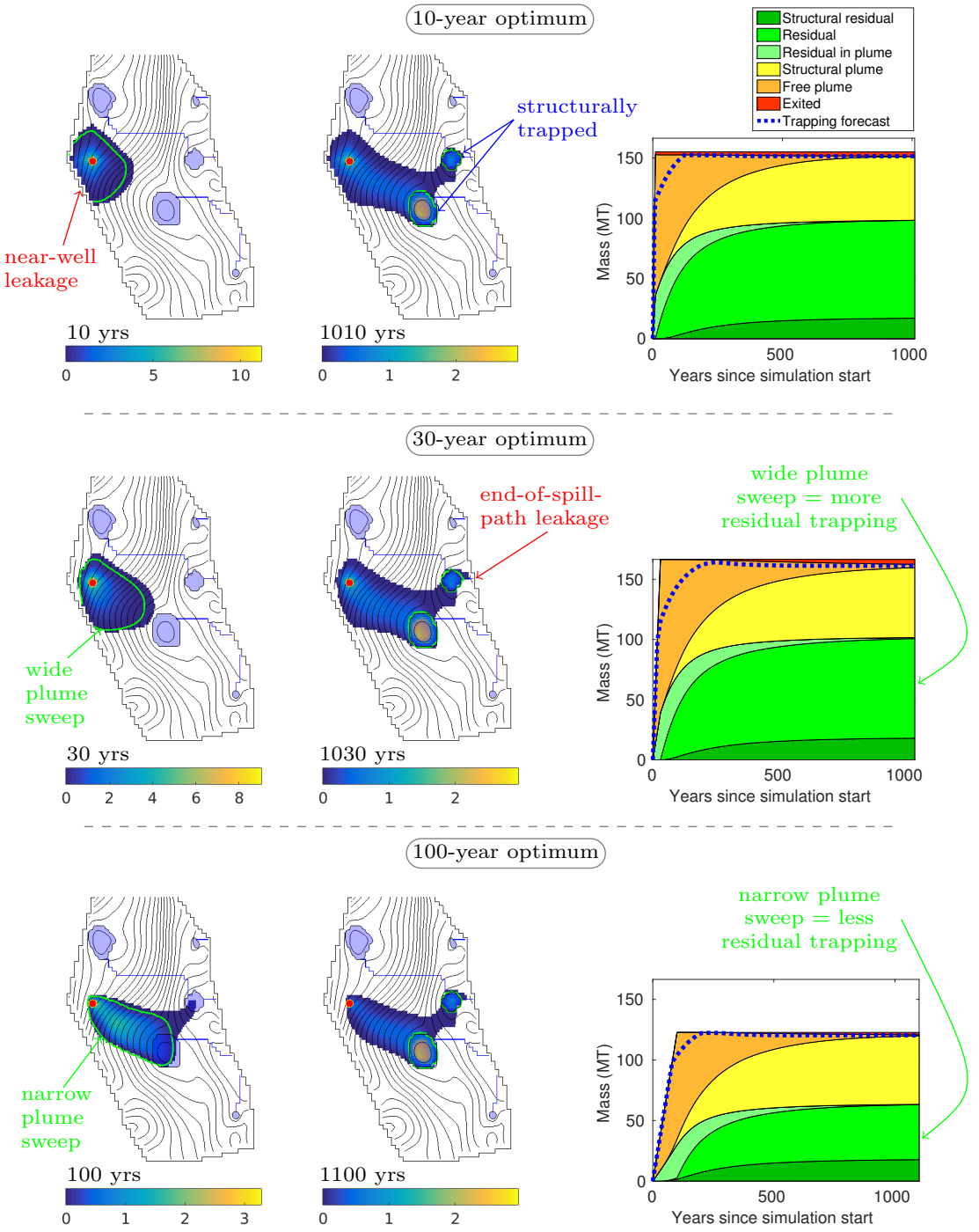

Fig. 5: Optimal solution given a 10-year, 30-year, and 100-year injection period, for a single-well scenario in Sleipner. *Left to right*: CO_2 saturations at end of injection period and after 1000 years of post-injection, and trapping inventories. Well location is indicated by red dot, and is identical in all three cases. Colorbars refer to tonnes of CO_2 per lateral square meter.

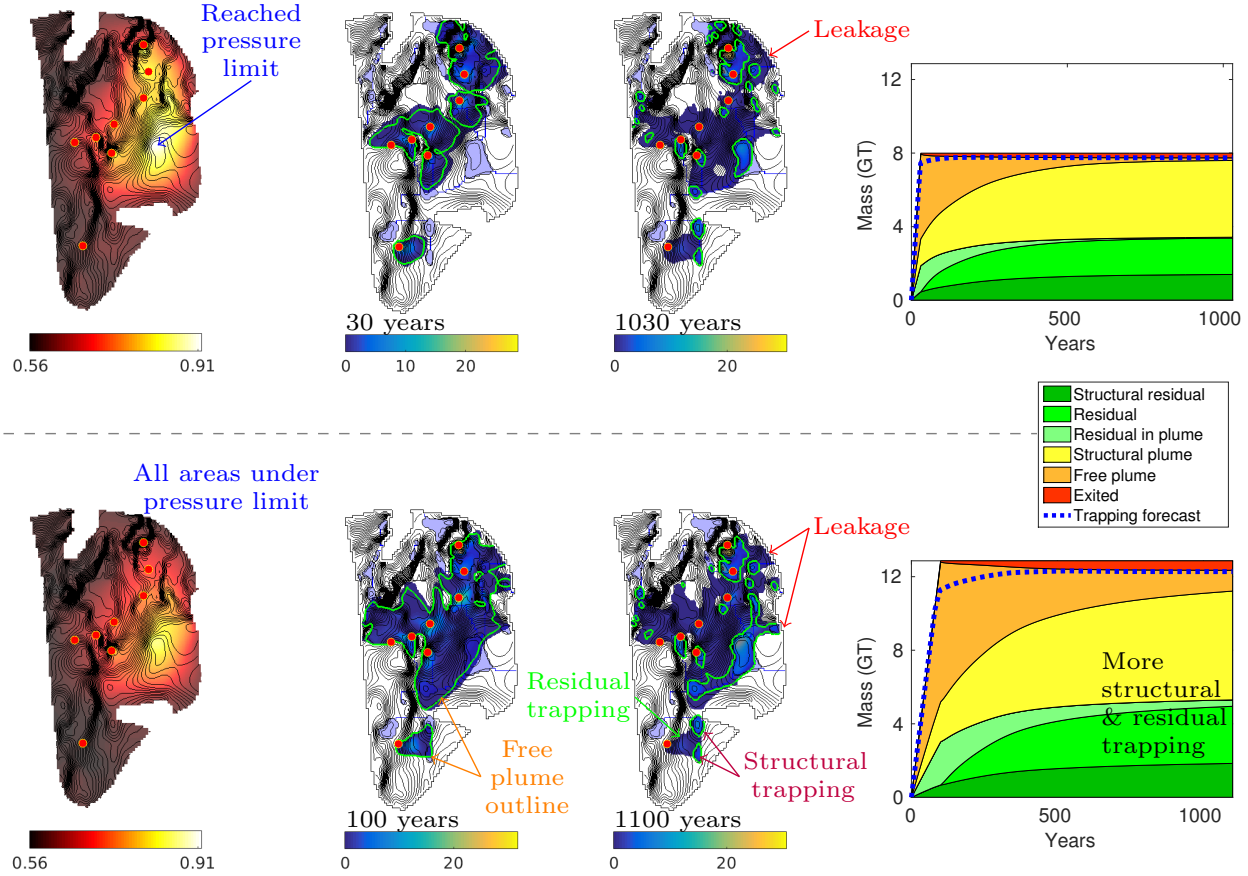

Fig. 6: Comparison of the optimal solutions given a 30-year (top row) and 100-year (bottom row) injection period in Brent. *Left to right*: fraction of overburden pressure reached, CO_2 saturations at end of injection and end of simulated period, and trapping inventory. Saturation colorbars refer to tonnes of CO_2 per lateral meter squared. Predefined pressure limit is 0.9 times overburden pressure.

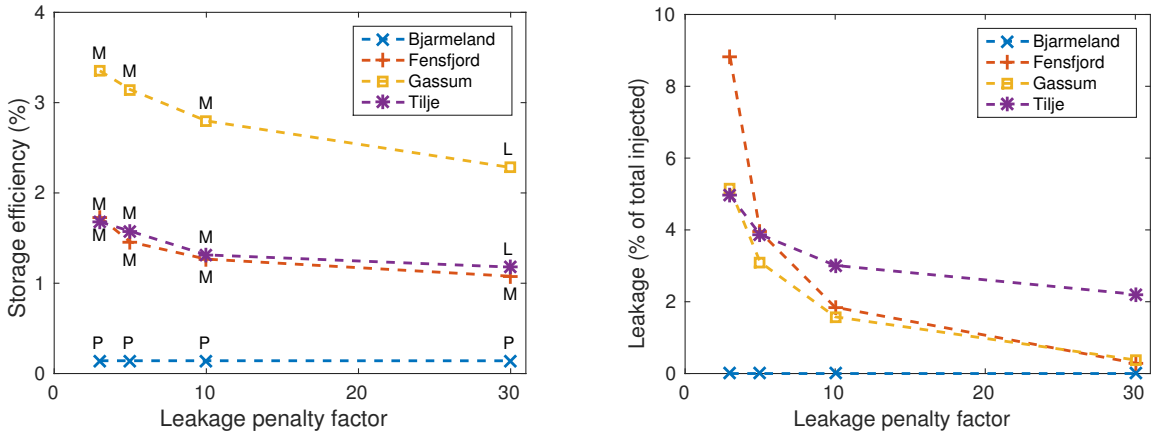

Fig. 7: Impact of leakage penalty factor on the optimized storage efficiency (left) and amount of leakage (right) of select formations. Storage limitation due to leakage, pressure, or a combination of both are indicated by labels “L”, “P”, and “M”, respectively.

the CO_2 plume, thus reducing the amount of CO_2 that reaches the formation boundaries. As such, we can expect to find that more of the storage efficiencies will be limited due to injectivity issues or pressure buildup rather than due to leakage. Also, our assumption of open boundaries with hydrostatic pressure likely had an influence on the degree of simulated leakage. In reality, a certain amount of resistance to flow across the open boundaries exists, however the precise nature of this fluid exchange remains uncertain without knowledge of the geology beyond the formation boundary. Despite all of the above mentioned limitations, our proposed method of categorization is still applicable should we include more petrophysics and geological detail. Investigating the impact of boundary conditions, as well as properly accounting for the formations which are considered to be closed aquifer systems, is left for future work.

Acknowledgements

This work was funded in part by the Research Council of Norway through grant no. 243729 (Simulation and optimization of large-scale, aquifer-wide CO_2 injection in the North Sea).

References

[1] U.S. Department of Energy, Office of Fossil Energy, Carbon Storage Atlas, 5th Edition, netl.doe.gov/File Library/Research/Coal/carbon-storage/atlasv/ATLAS-V-2015.pdf (2015).
[2] S. Bachu, Review of CO2 storage efficiency in deep saline aquifers, Int. J. Greenh. Gas Con. 40 (2015) 1–15. doi:10.1016/j.ijggc.2015.01.007.
[3] S. Bachu, A. Melnik, R. Bistran, Approach to evaluating the CO2 storage capacity in Devonian deep saline aquifers for emissions from oil sands operations in the Athabasca area, Canada, Energy Procedia 63 (2014) 5093–5102. doi:10.1016/j.egypro.2014.11.539.
[4] B. E. Bradshaw, L. K. Spencer, A.-L. Lahtinen, K. Khider, D. J. Ryan, J. B. Colwell, A. Chirinos, J. Bradshaw, J. J. Draper, J. Hodgkinson, M. McKillop, An assessment of Queensland's CO2 geological storage prospectivity–The Queensland CO2 geological storage atlas, Energy Procedia 4 (2011) 4583–4590. doi:10.1016/j.egypro.2011.02.417.
[5] M. Cloete, Atlas on geological storage of carbon dioxide in South Africa, Tech. rep., Council for Geoscience, Johannesburg, South Africa, sacccs.org.za/wp-content/uploads/2010/11/Atlas.pdf (2010).
[6] D. Lewis, M. Bentham, T. Cleary, R. Vernon, N. O'Neill, K. Kirk, A. Chadwick, D. Hilditch, K. Michael, G. Allinson, P. Neal, M. Ho, Assessment of the potential for geological storage of carbon dioxide for the island of Ireland, Tech. rep., Sustainable Energy Ireland, Environmental Protection Agency, Geological Survey of Northern Ireland, and Geological Survey of Ireland, seai.ie/News-Events/Press-Releases/Storage-of-CO2-Report-Sept-08.pdf (2008).
[7] F. E. Watson, S. A. Mathias, S. E. Daniels, R. R. Jones, R. J. Davies, B. J. Hedley, J. van Hunen, Dynamic modeling of a UK North Sea saline formation for CO2 sequestration, Petrol. Geosci. 20 (2) (2014) 169–185. doi:10.1144/petgeo2012-072.
[8] M. Bentham, T. Mallows, J. Lowndes, A. Green, CO2 STORage Evaluation Database (CO2 Stored): The UK's online storage atlas, Energy Procedia 63 (2014) 5103–5113. doi:10.1016/j.egypro.2014.11.540.
[9] E. K. Halland, J. Mujezinović, F. Riis (Eds.), CO_2 Storage Atlas: Norwegian Continental Shelf, Norwegian Petroleum Directorate, 2014, npd.no/en/Publications/Reports/Compiled-CO2-atlas.
[10] R. Bøe, C. Magnus, P. T. Osmundsen, B. I. Rindstad, CO2 point sources and subsurface storage capacities for CO2 in aquifers in Norway, Tech. rep., Geological Survey of Norway, Trondheim, ngu.no/FileArchive/101/2002 010 skjerm.pdf (2002).
[11] Geological Survey of Denmark and Greenland, Nordic CO2 storage atlas, data.geus.dk/nordiccs/.
[12] E. Lindeberg, J. F. Vuillaume, A. Ghaderi, Determination of the CO2 storage capacity of the Utsira formation, Energy Procedia 1 (1) (2009) 2777–2784. doi:10.1016/j.egypro.2009.02.049.
[13] V. T. H. Pham, F. Riis, I. T. Gjeldvik, E. K. Halland, I. M. Tappel, P. Aagaard, Assessment of CO2 injection into the south Utsira-Skade aquifer, the North Sea, Norway, Energy 55 (2013) 529–540. doi:10.1016/j.energy.2013.03.026.
[14] F. Riis, E. Halland, CO2 Storage Atlas of the Norwegian Continental Shelf: Methods Used to Evaluate Capacity and Maturity of the CO2 Storage Potential., Energy Procedia 63 (2014) 5258–5265. doi:10.1016/j.egypro.2014.11.557.
[15] A. E. Lothe, B. Emmel, A. Grøver, P. E. Bergmo, CO2 storage modelling and capacity estimation for the Trøndelag platform, offshore Norway - using a basin modelling approach, Energy Procedia 63 (2014) 3648–3657. doi:10.1016/j.egypro.2014.11.394.
[16] G. T. Eigestad, H. K. Dahle, B. Hellevang, F. Riis, W. T. Johansen, E. Øian, Geological modeling and simulation of CO2 injection in the Johansen formation, Comput. Geosci. 13 (4) (2009) 435–450. doi:10.1007/s10596-009-9153-y.
[17] H. Class, A. Ebigbo, R. Helmig, H. K. Dahle, J. M. Nordbotten, M. A. Celia, P. Audigane, M. Darcis, J. Ennis-King, Y. Fan, B. Flemisch, S. E. Gasda, M. Jin, S. Krug, D. Labregere, A. Naderi Beni, R. J. Pawar, A. Sbai, S. G. Thomas, L. Trenty, L. Wei, A benchmark study on problems related to CO2 storage in geologic formations, Comput. Geosci. 13 (4) (2009) 409–434. doi:10.1007/s10596-009-9146-x.
[18] H. M. Nilsen, K.-A. Lie, O. Møyner, O. Andersen, Spill-point analysis and structural trapping capacity in saline aquifers using MRST-co2lab, Computers & Geosciences 75 (2015) 33–43. doi:10.1016/j.cageo.2014.11.002.
[19] K.-A. Lie, H. M. Nilsen, O. Andersen, O. Møyner, A simulation workflow for large-scale CO2 storage in the Norwegian North Sea, Comput. Geosci. 20 (3) (2016) 607–622. doi:10.1007/s10596-015-9487-6.
[20] J. M. Nordbotten, M. A. Celia, Geological Storage of CO2: Modeling Approaches for Large-Scale Simulation, John Wiley & Sons, Inc., 2012.

[21] P. Wolfe, Convergence conditions for ascent methods, SIAM Rev. 11 (2) (1969) 226–235. doi:10.1137/1011036.
[22] P. Wolfe, Convergence conditions for ascent methods. II: Some corrections, SIAM Rev. 13 (2) (1971) 185–188. doi:10.1137/1013035.
[23] J. D. Jansen, Adjoint-based optimization of multi-phase flow through porous media – a review, Computers & Fluids 46 (1) (2011) 40–51, 10th ICFD Conference Series on Numerical Methods for Fluid Dynamics (ICFD 2010). doi:10.1016/j.compfluid.2010.09.039.
[24] O. Andersen, H. M. Nilsen, K.-A. Lie, Reexamining CO2 storage capacity and utilization of the Utsira Formation, in: ECMOR XIV – 14th European Conference on the Mathematics of Oil Recovery, Catania, Sicily, Italy, 8-11 September, EAGE, 2014. doi:10.3997/2214-4609.20141809.
[25] H. M. Nilsen, K.-A. Lie, O. Andersen, Analysis of CO2 trapping capacities and long-term migration for geological formations in the Norwegian North Sea using MRST-co2lab, Computers & Geosciences 79 (2015) 15–26. doi:10.1016/j.cageo.2015.03.001.
[26] O. Andersen, K.-A. Lie, H. M. Nilsen, An open-source toolchain for simulation and optimization of aquifer-wide CO2 storage, Energy Procedia 86 (2016) 324–333. doi:10.1016/j.egypro.2016.01.033.
[27] R. Allen, H. M. Nilsen, O. Andersen, K.-A. Lie, On obtaining optimal well rates and placment for CO2 storage, in: ECMOR XV – 15th European Conference on the Mathematics of Oil Recovery, Amsterdam, Netherlands, 29 August – 1 September, EAGE, 2016. doi:10.3997/2214-4609.201601823.